Computational Neuroscience:
Realistic Modeling for Experimentalists
Erik De Schutter (Editor)
R.C. Cannon (CD-ROM)
CRC-Press, 2001, Boca Raton, USA

Chapter 7

Modeling dendritic geometry and the development of nerve connections

Jaap van Pelt, Arjen van Ooyen, Harry B.M. Uylings

Preprint

Chapter 7

Modeling dendritic geometry and the development of nerve connections

Jaap van Pelt, Arjen van Ooyen, Harry B.M. Uylings

Graduate School Neurosciences Amsterdam, Netherlands Institute for Brain Research, Meibergdreef 33, 1105 AZ Amsterdam, The Netherlands

Correspondence to:

Dr. Jaap van Pelt
Netherlands Institute for Brain Research
Meibergdreef 33, 1105 AZ Amsterdam
The Netherlands
Phone: (31) 20 5665481; Fax: (31) 20 6961006
E-mail: J.van.Pelt@nih.knaw.nl

Contents

INTRODUCTION

The two methods described in this chapter focus on the development of neuronal geometry and interneuronal connectivity. The first *model for dendritic geometry* is based on a stochastic description of elongation and branching during neurite outgrowth. This model allows the user to generate random trees by means of (Monte Carlo) computer simulations. Using optimized parameters for particular neuron types, the geometrical properties of these modeled trees can be made to correspond with those of the empirically observed dendrites. The second *model for the development of nerve connections* describes competition for neurotrophic factors. This

model is formulated in terms of differential equations which can be studied analytically using well-known tools for nonlinear system analysis.

7.1 MODELING DENDRITIC GEOMETRY

Interest in the geometry of dendritic branching patterns stems from a variety of reasons. Anatomists are interested in the morphological characterization and differences among neuronal classes as well as in the morphological variations within these classes. Developmental neuroscientists seek to discover the rules of development and the mechanisms by which neurons attain their final morphological appearence. Physiologists are interested in how dendritic morphology is involved in synaptic connectivity within neuronal networks, and in the integration and processing of postsynaptic potentials. Computer scientists are interested in algorithms for generating tree structures. The enormous amount of structural and functional variation with which nature confronts us is a major challenge providing strong motivation to search for 'fundamental rules' or minimal parsimonious descriptions of architecture, development and function. Modeling the geometry of dendritic branching patterns can provide answers to a variety of morphological, physiological and developmental questions and a variety of approaches have been developed. In these modeling approaches, a distinction can be made between reconstruction and growth models.

Reconstruction models use the abstracted geometrical properties of a set of observed trees, and provide algorithms for randomly generating trees with identical statistical geometrical properties. A typical example is given by the work of Burke et al. [1], who developed a parsimonious description on the basis of empirically obtained distribution functions for the length and diameters of dendritic branches and for the diameter relations at bifurcation points. Random dendrites are generated by a repeated process of random sampling of these distributions in order to decide whether or not a traced neurite should branch, and for obtaining the diameters of the daughter branches. The modeled dendrites obtained in this way conform to the original distribution functions of shape characteristics. An important assumption in this approach is that the sampled shape properties are independent from each other. Hillman [2] emphasized the statistical correlation of segment diameters across branch points and their relation to segment lengths as fundamental parameters of neuronal shape. Tamori [3] postulated a principle of least effective volume in deriving equations for dendritic branch angles. A sophisticated implementation of the reconstruction approaches by Hillman, Tamori and Burke has recently been developed by Ascoli et al. [4] in L-neuron, a modeling tool for the efficient generation and parsimonious description of dendritic morphology (URL: http://www.krasnow.gmu.edu/L-neuron/index.html). This modeling tool implements local and recursive stochastic and statistical rules into the formalism of L-systems. Kliemann [5] followed a different approach by considering all the segments at a given centrifugal order as individuals of the same generation, which may or may not give rise to individuals in a subsequent generation (by producing a bifurcation point with two daughter segments). Mathematically, such a dendritic reconstruction can be described by a *Galton-Watson process*, based on empirically obtained splitting probabilities for defining per generation whether a segment will be a terminal or an intermediate one. Applications of this method to dendrites grown in vitro can be found in e.g., [6].

Growth models, in contrast, aim at revealing rules of neuronal growth in relation to the geometrical properties of the trees emerging from these rules. The outgrowth of neurons proceeds by the dynamic behavior of growth cones, specialized structures at the tips of outgrowing neurites which mediate neuritic elongation and branching (e.g., [7]). Mature neurons have attained their morphological features as result of this process. Growth models include these processes of elongation and branching. Several implementations have been studied, differing in the level of detail of the mechanisms involved. *Topological growth models* focus on the branching process only and ignore all metrical aspects of dendrites. They have shown how the probability of occurrence of topologically different tree types depends on the rules for outgrowth. These rules include, for instance, (1) growth by sequential or synchronous branching and (2) random selection of segments participating in the branching process, based on uniform or order-and type-dependent branching probabilities. Examples of such topological approaches are in [8, 9, 10] and in [11] for a review. *Metrical growth models* include rules for both branching and elongation of segments. These models allow the study of both metrical and topological properties of the generated dendrites, in relation to the growth assumptions, and have been developed by e.g., [12, 13, 14, 11].

The studies reviewed above concern *phenomenological approaches* in the sense that both the reconstruction and the growth models are based on simple probabilistic schemes, still aiming at the reproduction of the empirically obtained geometrical characteristics. A point of distinction is that the growth models are based on a developmental process in time and as such are able to include mechanisms that depend on time, and on the growing tree itself, such as its size. Reconstruction models do not include this dimension, and the underlying probabilistic schemes are based on empirical correlation and distribution functions of the shape parameters of particular sets of trees. Growth models should, in principle, be able to describe groups of trees, reconstructed at different time points during development, using the same set of parameters. Reconstruction models, however, may need different sets of optimized parameter values for each age groups. Additional to these phenomenological approaches, models have been and are being developed which include more detailed intracellular and local environmental mechanisms and processes in dendritic growth models. Such biophysical and biochemical processes concern, for instance, the polymerization of the intracellular cytoskeleton [15]) and neuritic tension and lateral inhibition (e.g., [14]).

The growth model described in this chapter includes branching and elongation as stochastic processes. The stochasticity assumption is based on the notion that the actual behavior of growth cones, mediating elongation and branching, is subject to so many intracellular and extracellular mechanisms that a probabilistic description is appropriate. The stochasticity assumption, thus, does not imply that the processes involved are stochastic by themselves, but only that their outcome can be described as such. The model has a modular structure, evolved in the course of time by separately studying the branching process (a) with respect to the choices of the segments at which branching events occur, (b) with respect to the time pattern of the branching events, and (c) by finally including the elongation of the segments. Each phase was validated by comparison with specific empirical findings. The modular structure of the model facilitates the optimization of the model parameters, which will be illustrated in this chapter. The model allows the generation of random dendritic trees, and it will be shown how these trees conform in their geometrical properties to empirical observations. This will be illustrated for a set of rat cortical pyramidal cell basal dendrites and for a small set of

three cerebellar Purkinje cell dendritic trees from the guinea pig.

7.1.1 Geometry of dendritic trees

Typical shape characteristics of dendritic trees are: the *number* of terminal tips (degree) or branch points; the *lengths and diameters* of the segments between these branch points and tips; and the *connectivity pattern* of the segments (topological structure). A distinction is made between *terminal* segments (ending in tips) and *intermediate* segments (ending in a branch point) (Fig. 7.1). Related shape properties are *path lengths* (total length of the path from the dendritic root to a branch point or terminal tip) and the number of segments at a particular centrifugal order. The *centrifugal order* of a segment is equal to the number of branch points on the path from the dendritic root up to the segment, thus indicating the position of the segment in the tree. The embedding of the segments in 3D space and their irregular shapes, although prominent features of dendritic trees, are not dealt with in this chapter. The *topological asymmetry* of a given tree α^n with n terminal segments will be quantified by means of the *tree asymmetry index* A_t defined as

$$A_t(\alpha^n) = \frac{1}{n-1} \sum_{j=1}^{n-1} A_p(r_j, s_j),$$

being the mean value of all the $n-1$ *partition asymmetries* $A_p(r_j, s_j)$ in the tree. Partition asymmetries indicate, at each of the $n-1$ bifurcation points, the relative difference in the number of bifurcation points $r_j - 1$ and $s_j - 1$ in the two subtrees emerging from the jth bifurcation point. [11] The *partition asymmetry* A_p at a bifurcation is defined as $A_p(r, s) = |r-s|/(r+s-2)$ for $r+s > 2$, with r and s denoting the number of terminal segments in the two subtrees. $A_p(1, 1) = 0$ by definition. Note that a binary tree with n terminal segments has $n-1$ bifurcation points. The elements of a tree are further illustrated in Fig. 7.1.

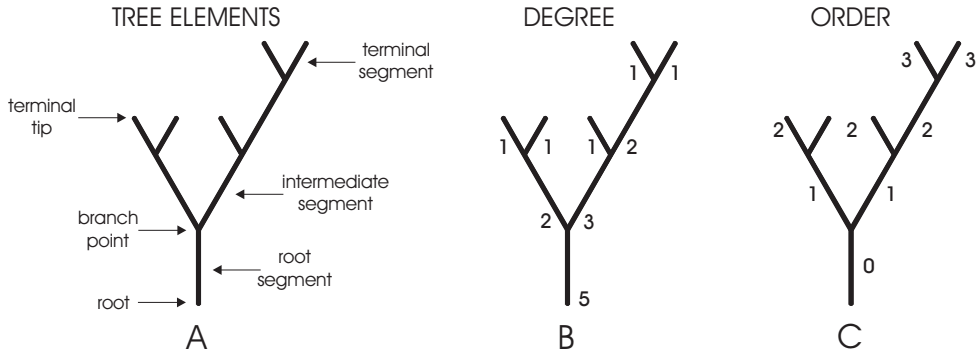

Figure 7.1 (A) Elements of a topological tree, with a distinction of branch points, terminal tips and root, intermediate and terminal segments. Segments are labeled according to (B) the number of tips in their subtrees (degree) and (C) their distance from the root (centrifugal order).

7.1.2 Dendritic growth model - assumptions

Basic actions in the growth model are elongation and branching of segments, assumed to be independent stochastic processes in time. At each branching event a bifurcation is formed

at the tip of a terminal segment, from which two new daughter terminal segments emerge. Elongation is assumed to occur at terminal segments only. The branching probability of a terminal tip is assumed to depend on the momentary number of tips in the growing tree and on its position in the tree. The branching process results in a proliferation of tips and this process fully determines the final variation among dendritic trees with respect to the number of terminal segments. The branching parameters can be derived from the shape of empirical terminal segment number distributions. The topological structure of a fully grown dendrite is determined by the sequence of particular segments at which branching occurs. The segment lengths are determined both by the elongation rates of the segments and by the elapsed time between successive branching events. Segment length distributions can therefore only be studied once the branching process has been optimized. No developmental rules have been incorporated for the diameter of segments. Rather, these diameters will be assigned to the segments once the skeleton tree has been grown.

7.1.3 Dendritic growth model - equations

7.1.3.1 Branching process - describing the variation in the number of segments and the variation in topological tree types

First, we describe the branching process on a series of time-bins, without specifying explicitly the duration of each bin. The branching probability of a terminal segment at time bin i is given by

$$p_i = C2^{-S\gamma}B/Nn_i^E, \tag{7.1}$$

with N denoting the total number of time bins in the full period of development and n_i denoting the actual number of terminal segments or tips (degree) in the tree at time bin i. [10] The parameter B denotes the expected number of branching events at an isolated segment in the full period, while parameter E determines how strongly the branching probability of a terminal segment depends on the number of tips in the tree. Such a dependency turns out to be essential for reducing the proliferating effect of the increasing number of tips on the total branching rate of the tree. [10] Parameter γ denotes the centrifugal order of the terminal segment while

$$C = n/\sum_{j=1}^{n} 2^{-S\gamma_j}$$

is a normalization constant, with a summation over all n terminal segments. Parameter S determines how strongly the branching probability of a terminal segment depends on the proximal/distal position of the segment in the tree. For $S = 0$, all terminal segments have equal probabilities for branching, a mode of growth called random terminal growth. The frequency distribution of tree types produced by this mode of growth has an expected value for the tree asymmetry index of 0.46 for large trees. [11] For $S \neq 0$, the branching probability of a segment depends on its position in the tree, resulting in more symmetrical trees when $S > 0$ and more asymmetrical trees when $S < 0$. The number of time bins N can be chosen arbitrarily, but such that the branching probability per time bin remains much smaller than

unity, making the probability of there being more than one branching event in a given time bin negligibly small.
The distribution of the number of terminal segments in dendritic trees after a period of growth can be calculated by means of the recurrent expression

$$P(n,i) = \sum_{j=0}^{n/2} P(n-j, i-1) \begin{pmatrix} n-j \\ j \end{pmatrix} [p(n-j)]^j \, [1-p(n-j)]^{n-2j}, \tag{7.2}$$

with $P(n,i)$ denoting the probability of a tree of *degree* n at time bin i with $P(1,1) = 1$, and $p(n)$ denoting the branching probability per time-bin of a terminal segment in a tree of *degree* n, with $p(n) = B/Nn^E$. [10] A tree of *degree* n at time-bin i emerges when j branching events occur at time-bin $i-1$ in a tree of *degree* $n-j$. The recurrent equation expresses the probabilities of all these possible contributions from $j = 0, ..., n/2$. The last two terms express the probability that, in a tree of *degree* $n-j$, j terminal segments will branch while the remaining $n-2j$ terminal segments will not do so. The combinatorial coefficient $\begin{pmatrix} n-j \\ j \end{pmatrix}$ expresses the number of possible ways of selecting j terminal segments from the existing $n-j$ ones.

7.1.3.2 Elongation process - describing the variation in segment lengths

Elongation was initially included in the branching model by assigning an elongation rate to growth cones at the time of their birth (i.e. after a branching event) which was randomly chosen from a predefined distribution. This implementation was successful in describing the mean and standard deviation of segment length distributions of basal dendrites of rat cortical pyramidal neurons. [10] This agreement with empirical data was obtained by additionally assuming that the elongation rate differed during two phases of dendritic development, the first with branching and elongation, the second with elongation only.
Recent studies have also focussed on the shape of the segment length distributions, showing that the first implementation of the elongation process resulted in monotonically decreasing length distributions for intermediate segments. Empirical distributions of different cell types, however, consistently show intermediate segment length distributions with a modal shape. (e.g., [13, 16] In reconstructions of stained neurons short intermediate segments apparently occur less frequently than was expected. Nowakowski et al. first noticed this phenomenon and suggested a transient suppression of the branching probability immediately after a branching event. [13] Such a reduction indeed resulted in a correct shape for the intermediate segment length distributions. [13] Implementing such an assumption in our approach has a drawback, however, in that it interferes with the branching process as described by the parameters B and E and consequently with the shape of the degree distribution. We therefore followed a different approach by giving daughter segments an initial length immediately after a branching event, and letting them further elongate at a slower rate. The elongation process is then split into a process associated with a branching event, and a subsequent elongation process. Such an implementation becomes plausible by considering that a branching event is not a point process in time, but rather proceeds during a certain period of time during which a growth cone splits and the daughter branches become stabilized.

7.1.3.3 Time

Continuous time enters into the model when elongation rates are used. Thus far, the branching process (and the associated initial segment length assignments) were defined on a series of time bins, without specifying the time bin durations. For the mapping of the time bins onto real time, the total duration of the branching and elongation period needs to be defined as well as the type of mapping, which we will assume to be linear.
It will be shown in the examples in this chapter that these assumptions indeed result in a correct description of the segment length distribution while maintaining the proper shape of the degree distribution. The initial length, given to new daughter segments, is determined by random sampling of a predefined distribution. Both for the elongation rate and for the initial length we have chosen a gamma distribution. Such a distribution is expected for distances between Poisson distributed branching events along the path of an outgrowing neurite. [17]

Box 7.1 The Gamma Distribution
A gamma distribution has the form

$$g(x;\alpha,\beta,\gamma) = \frac{1}{\beta^{\gamma}\Gamma(\gamma)} e^{\frac{x-\alpha}{\beta}} (x-\alpha)^{\gamma-1} \tag{7.3}$$

for $x > \alpha$, $\beta > 0$, $\gamma > 0$, while the gamma function $\Gamma(\gamma)$ is defined by $\Gamma(\gamma) = \int_0^{\infty} e^{-t} t^{\gamma-1} dt$. [18] The cumulative distribution is given by $G(x;\alpha,\beta,\gamma) = \int_{\alpha}^{x} g(x;\alpha,\beta,\gamma)dt$ with $G(\infty;\alpha,\beta,\gamma) = 1$. Parameter α indicates the start of the distribution (offset), β a scaling unit and γ the shape of the distribution. The mean value of the distribution is given by $\overline{x} = \alpha + \beta\gamma$ and the standard deviation is given by $\sigma_x = \beta\sqrt{\gamma}$. The modus of the distribution is at $x = \alpha + \beta(\gamma - 1)$. For a given choice of the offset α, the parameters β and γ can be estimated from the mean and standard deviation of a distribution by

$$\beta = \frac{\sigma^2}{\overline{x} - \alpha} \qquad \text{and} \qquad \gamma = \frac{\sigma^2}{\beta^2} = \left(\frac{\overline{x} - \alpha}{\sigma}\right)^2. \tag{7.4}$$

For ease of interpretation, we will characterize a gamma function by the parameters α, $\overline{x}$ and σ_x.

7.1.3.4 Segment diameter

Segment diameters have not been modeled as part of the growth process, but are assigned to the skeleton of the full grown tree. A power law relationship will be assumed, relating the diameters of the segments at a branch point. By the power law relation, the diameter of a parent segment (d_p) relates to the diameter of its daughter segments d_1 and d_2 as

$$d_p^e = d_1^e + d_2^e, \tag{7.5}$$

with e denoting the branch power exponent. According to this relation, the diameter of an intermediate segment d_i relates to the number n and diameter d_t of the terminal segments in its subtree as $d_i = n^{1/e} d_t$, independent of the topological structure of the subtree.

7.1.4 Dendritic growth model - parameters

The model includes the parameters B, E and S defining the branching process; the parameters $\alpha_{l_{in}}$, $\overline{l_{in}}$ and $\sigma_{l_{in}}$ defining the offset, mean and standard deviation, respectively, of the gamma distribution $g_{l_{in}}$ for the initial lengths; and the parameters α_v, $\overline{v}$ and σ_v defining the offset, mean and standard deviation, respectively, of the gamma distribution for the sustained elongation rates. At a branching event, initial lengths are assigned to both newly formed daughter segments, by drawing random samples from the initial length distribution $g_{l_{in}}$, and elongation rates are assigned to both daughter segments, by drawing random samples from an elongation rate distribution g_v. These elongation rates hold until new branching events occur at the respective segments. Associated with the sustained elongation we need to specify the duration of the period of branching and elongation T_{be} and of the subsequent period of elongation only T_e.

7.1.4.1 Parameter estimation

A summary of the parameters in the dendritic growth model is given in Table 7.1. Finding the optimal parameter values needed to describe a particular set of observed dendritic branching patterns is a multidimensional optimization task. The modular character of the model and the assumption of independent branching and elongation, however, make it possible to optimize branching and elongation processes separately. Plots of shape properties versus parameter values offer additional material for manually finding reasonable parameter estimates. This will be described below.

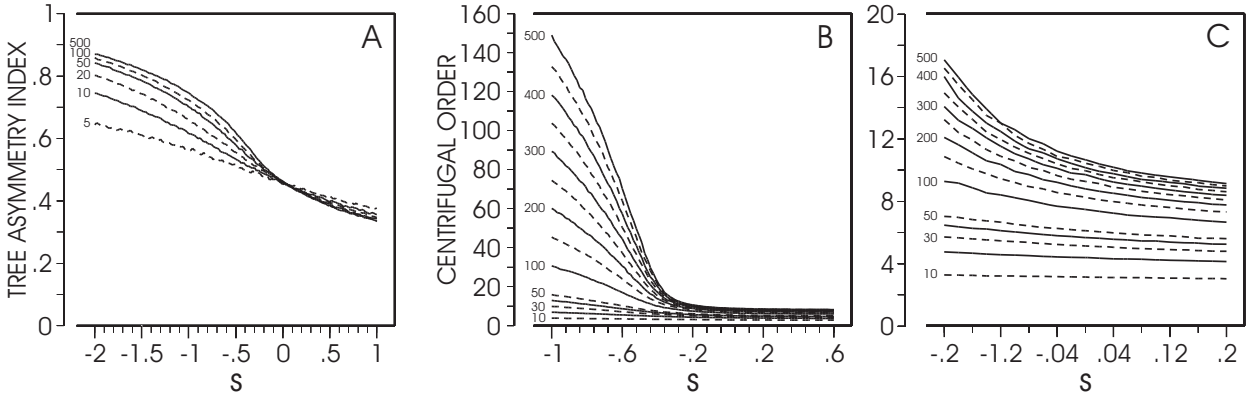

Figure 7.2 (A) Expected value of the tree asymmetry index for a set of trees as a function of the growth parameter S, calculated for trees of degree 5, 10, 20, 50, 100, 500, and (B) mean value of the centrifugal order of segments as a function of the growth parameter S, calculated for trees of degree 10, 20, 30, 40, 50, 100, 150, 200, 250, 300, 350, 400, 450 and 500. Panel (C) expands the area -0.2 < S < 0.2.

Parameter S - Parameter S can be estimated from the value of the topological asymmetry index. Fig. 7.2A illustrates how the expected value of the asymmetry index depends on the value of parameter S and the number of terminal segments in the tree. The equations used to calculate the tree-asymmetry index are reviewed in [11]. Note that these equations are derived for the more general case in which also intermediate segments may branch. In the present study we assume terminal branching only. Alternatively, parameter S can also be

estimated from the mean centrifugal order of the tree. Figures 7.2B and C show how the mean centrifugal order depends on the parameter S and the number of terminal segments in the trees.

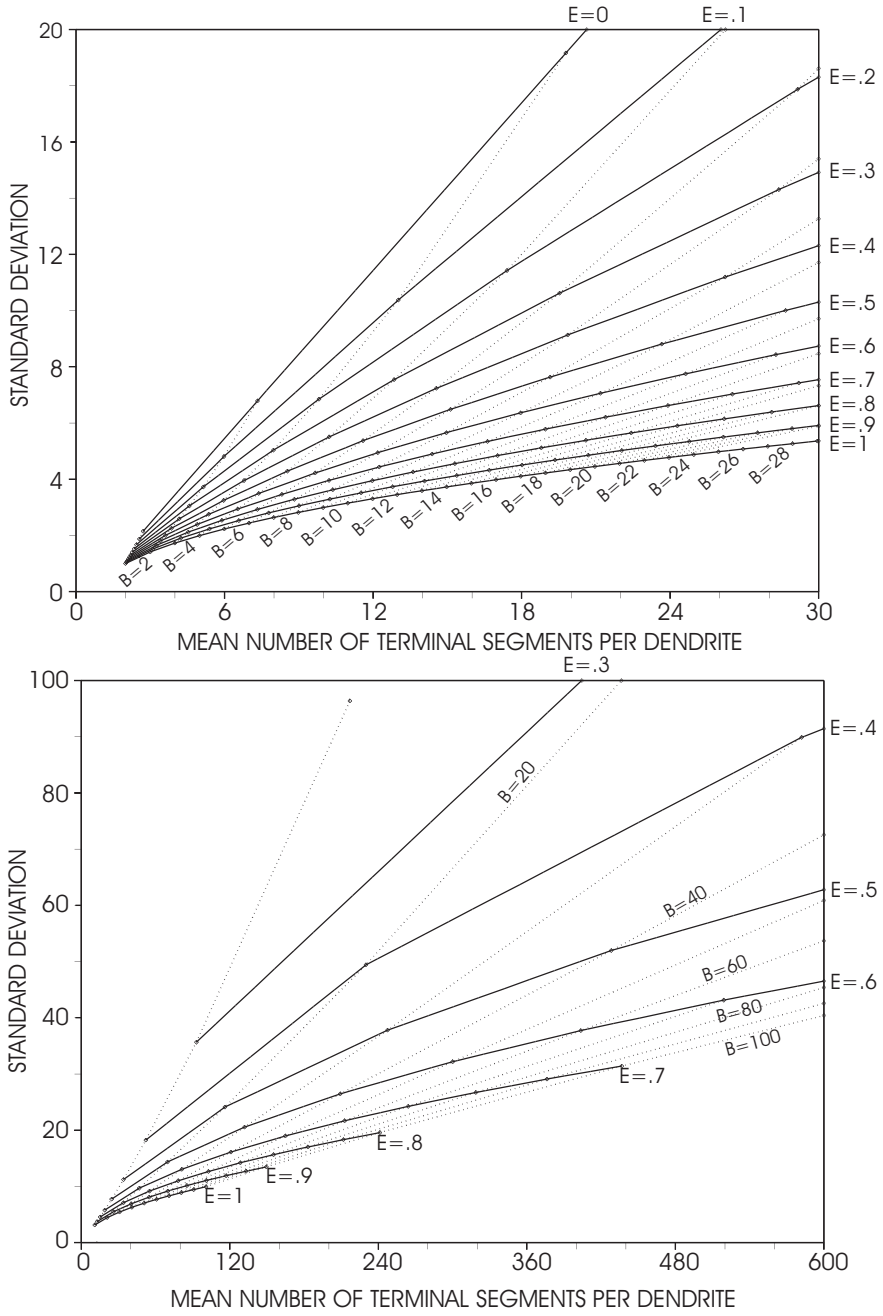

Figure 7.3 Mapping of the (B, E) parameter grid onto the $(mean, sd)$-plane. The map is obtained by calculating for many pairs of (B, E) model parameter values the mean and standard deviation of the degree distribution, as produced by the model, which are subsequently plotted as a point in the $(mean, sd)$-plane. The continuous lines connect points in the $(mean, sd)$-plane with equal E value, the dotted lines connect points with equal B value. The map is calculated for a fine (panel A) and a course degree (panel B) scale.

Parameters B and E - Parameters B and E can be estimated from Fig. 7.3, illustrating the mapping from branching parameters B and E to the expected mean and sd values of the predicted degree distribution. The estimation proceeds by plotting the observed mean and sd in the figure and finding the coordinates of this point in the B,E grid.

Metrical parameters $\alpha_{l_{in}}$, $\overline{l_{in}}$, $\sigma_{l_{in}}$ for the initial length and α_v, $\overline{v}$ and σ_v for the sustained elongation rate - Once the branching process is defined, we need further specification of the gamma distributions for the initial lengths $g_{l_{in}}$ and for the sustained elongation rates g_v. The parameters in both $g_{l_{in}}$ and g_v have to be estimated from the empirical intermediate and terminal segment length distributions, and the path length distribution. Good estimates are, however, not directly obtained from these distributions but require a process of optimization. Some considerations may help in finding reasonable estimates when using a manual approach. The length of intermediate segments in the model is determined by (1) the initial length assigned after a branching event, (2) the elongation rate assigned to this segment and (3) the time elapsing before the segment experiences the next branching event. A segment becomes a terminal segment when it fails to undergo branching before the end of the growth period.

Terminal segments are generally longer than intermediate segments, both when compared for the whole tree and when compared for a given centrifugal order within the tree. (e.g., [19, 20, 21]) Many dendritic trees also show a decrease of terminal segment length with increasing centrifugal order. (e.g., [19]) These findings can be explained by considering that terminal segments of a given centrifugal order have had more time, on the average, to elongate than have intermediate segments of similar order, and that this time decreases for increasing order. [17] This phenomenon occurs only when segments show sustained elongation in addition to the initial length assigned to the daughter segments after branching. The length difference in terminal segments of lowest and highest order can thus be used to obtain an estimate of the sustained elongation rate during the period of branching. In the examples described in section 2.6 we will see that rat neocortical pyramidal cell basal dendrites show such differences whereas guinea pig cerebellar Purkinje cells do not (see also Fig. 7.4). Terminal segments may become much longer than intermediate ones when dendritic development includes a period of branching and elongation, followed by a period of elongation only. Additionally, the elongation rates need not be equal during these two periods.

The variation in path lengths is the final outcome of all stochasticity in elongation and branching. The standard deviation of the path length distribution can be used to estimate the variation in the sustained elongation rates. These considerations help in estimating the parameters α_v, $\overline{v}$ and σ_v in the gamma function g_v. The modal shape of the intermediate segment length distribution is determined by the initial length distribution $g_{l_{in}}$ and the sustained elongation rate. Estimates for the parameters in $g_{l_{in}}$ have to be obtained using equations 7.4 for a given choice for the length offset α_{in} and considering the choices for the parameters in g_v.

Diameter parameters - The segment diameters in a tree have not been modeled as part of a developmental process but have been directly assigned to the full grown skeleton tree by means of the following procedure. First, terminal segment diameters d_t are assigned by random sampling the observed diameter distribution (or a normal distribution based on the observed mean-sd values). Then, traversing the tree centripetally, at each bifurcation the

diameter of the parent segment is calculated by means of Eq. 7.5, using (a) the diameters of the daughter segments and (b) a branch power value e obtained by randomly sampling the observed branch power distribution.

TABLE 7.1
Summary of parameters used in the dendritic growth model.

Parameter	Aspect of growth	Related to
B	basic branching parameter	segment number
E	size-dependency in branching	segment number
S	order-dependency in branching	topological structure
$\alpha_{l_{in}}$	initial length - offset	segment length
$\overline{l_{in}}$ (μm)	initial length - mean	segment length
$\sigma_{l_{in}}$	initial length - SD	segment length
$\alpha_{v_{be}}$	elongation in 'branching/elongation phase' - offset	segment length
$\overline{v_{be}}$ (μm/h)	elongation in 'branching/elongation phase' - mean rate	segment length
α_{v_e}	elongation in 'elongation phase' - offset	segment length
$\overline{v_e}$ (μm/h)	elongation in 'elongation phase' - mean rate	segment length
cv_v	coefficient of variation in elongation rates	segment length
$\overline{d_t}$ (μm)	terminal segment diameter - mean	segment diameter
σ_{d_t}	terminal segment diameter - SD	segment diameter
$\overline{e}$	branch power - mean	segment diameter
σ_e	branch power - SD	segment diameter

Note: Note that the segment diameter parameters are not part of the growth model, but used afterwards to assign diameter values to the skeleton trees, produced by the model.

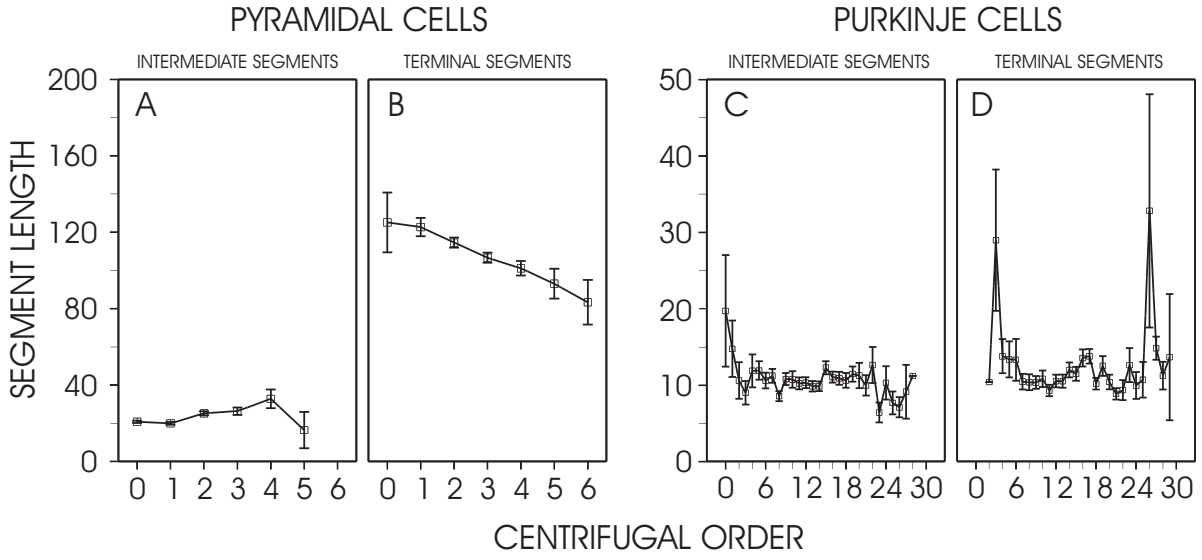

Figure 7.4 Length of intermediate and terminal segments plotted versus their centrifugal order, for S1-rat cortical layer 2/3 pyramidal cell basal dendrites (panels A and B) and for guinea pig cerebellar Purkinje cell dendritic trees (panels C and D).

7.1.5 Dendritic growth model - examples

7.1.5.1 Application to S1-rat cortical layer 2/3 pyramidal cell basal dendrites

In S1-rats, the outgrowth of the layer 2/3 pyramidal cell basal dendrites starts at about 1 day after birth and continues with branching and elongation up to about day 14, followed by a period of elongation up to about day 18. [16] The geometrical properties of these dendrites are given in Table 7.2 and the segment length distributions in Fig. 7.5 as hatched histograms. How segment lengths depend on centrifugal order is displayed in Fig. 7.4 (A,B).

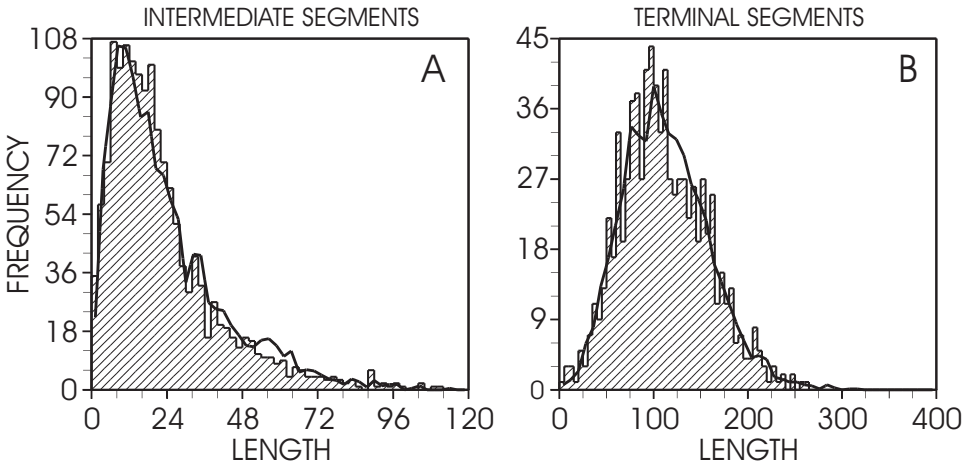

Figure 7.5 Comparison of (A) intermediate and (B) terminal segment length distributions of observed S1-rat cortical layer 2/3 pyramidal cell basal dendrites (hatched histograms) and model generated trees (continuous lines) for the parameter values given in Table 7.3.

Estimation of parameter S - Interpolation from the observed asymmetry index of 0.41 in Fig. 7.2A results in an estimate of S $\approx$ 0.5.
Estimation of parameters B **and** E - These parameters can be estimated from the mean and standard deviation of the observed degree distribution when plotted as the point (4.04, 2.04) in Fig. 7.3. Estimates of the corresponding coordinates in the B,E-grid are then obtained of $B = 2.52$ and $E = 0.73$.
Estimation of $g_{l_{in}}$ **and** g_v - The observed distribution of intermediate segment lengths (Fig. 7.5A) does not have a clearcut offset. We have assigned therefore a value of zero to the offset parameter α_{in}. The difference in length between highest and lowest order terminal segments is about 50 - 60 μm (Fig. 7.4B). Given a total duration of branching of 312 h (13 days), we obtain a rough estimate of ≈ 0.2 μm/h for the sustained elongation rate in the first developmental phase of branching and elongation. Values of $\overline{l_{in}} = 6$ μm and $\sigma_{l_{in}} = 5$ μm, for the initial length distribution in combination with a sustained mean elongation rate of 0.2 μm/h during this first phase, turned out to result in a good fit of the shape of the intermediate segment length distribution. The shape of the terminal segment length distribution was fitted

by assuming a mean elongation rate of 0.86 μm/h during the elongation phase. A coefficient of variation of 0.47 and a zero value for α_v were additionally assumed.

Diameter parameters - Diameter assignments can be made according to the procedure described in section 2.2, using parameter values $\overline{e} = 1.6$, $\sigma_e = 0.2$, $\overline{d_t} = 0.6$ μm and $\sigma_{d_t} = 0.1$. [2, 21]

TABLE 7.2
Comparison of shape properties from experimental observations of S1 rat cortical layer 2/3 pyramidal basal dendrites and of model simulated trees, obtained with optimized values of the growth parameters, as given in Table 7.3.

	Observed		Model predicted	
Shape parameter	**Mean**	**Standard deviation**	**Mean**	**Standard deviation**
Degree	4.04	2.04	4.05	2.02
Asymmetry index	0.41	0.24	0.4	0.23
Centrifugal order	1.86	1.2	1.85	1.19
Total dendritic length			527.6	265
Terminal length	110.7	45.2	112.62	44.8
Intermediate length	22.0	17.9	23.6	18.0
Pathlength	163.8	48.1	164.6	45.0

TABLE 7.3
Optimized values for growth parameters (see Table 7.1) to match the statistical shape properties of S1-rat cortical layer 2/3 pyramidal cell basal dendrites, given in Table 7.2.

Growth parameters										
B	E	S	α_{in}	$\overline{l_{in}}$ (μm)	$\sigma_{l_{in}}$	$\alpha_{v_{be}}$	$\overline{v_{be}}$ (μm/h)	α_{v_e}	$\overline{v_e}$ (μm/h)	cv_v
2.52	0.73	0.5	0	6	5	0	0.2	0	0.86	0.47

Note: Note that v_{be} and v_e define the sustained elongation rates during the first period of branching and elongation with a duration of 312 h (13 days), and the second period of elongation only with a duration of 96 h (4 days), respectively.

Statistical properties of model-generated trees - The shape properties of 10000 model trees are given by their mean and standard deviation and compared to experimental values in Table 7.2. An excellent match is obtained. Unfortunately, empirical data for the total dendritic length was not available. Not only the mean and standard deviation, but also the shapes of the distributions matched closely, as is seen in Fig. 7.5 for the length distributions of intermediate and terminal segments.

7.1.5.2 Application to guinea pig cerebellar Purkinje cell dendritic trees

The second example concerns the analysis of three guinea pig Purkinje cell dendritic trees, fully reconstructed by Rapp et al. [22] who analyzed in detail their physiological properties and made them available via the WWW (http://leonardo.ls.huji.ac.il/∼rapp). The geometrical properties of these cells have been calculated from these reconstructions, and their means and standard deviations are given in the 2nd and 3rd column of Table 7.4.

TABLE 7.4
Comparison of shape properties from experimental observations of guinea pig cerebellar Purkinje cell dendritic trees and of model simulated trees, obtained with optimized values of the growth parameters, as given in Table 7.5.

	Observed Trees 1+2+3		Model trees	
Shape parameter	**Mean**	**Standard deviation**	**Mean**	**Standard deviation**
Degree	436	31.8	436	32
Asymmetry index	0.5	0.01	0.49	0.02
Centrifugal order	13.7	5.1	13.8	5.9
Total length	9577	1105	9265	683
Terminal length	11.3	8.8	10.6	7.5
Intermediate length	10.6	7.5	10.6	7.6
Pathlength	189.3	64.1	166	66

Estimation of parameter S - Interpolation from the observed asymmetry index of 0.50 in Fig. 7.2A results in an estimate of $S \approx -0.15$. Interpolation from the observed mean centrifugal order of 13.7 in Fig. 7.2C results in an estimate of $S \approx -0.14$.
Estimation of parameters B **and** E - The values for the mean and standard deviation of the observed degree distribution (436, 31.8) form a point in the map in Figure 7.3. The B, E coordinates of this point can be obtained by reference to the B-E grid. A manual estimate of $B = 95$ and $E = 0.69$ has been used. Note that the mean and standard deviation of the degree distribution are based on only three observations. More observations are needed in order to obtain a stable estimate for the location of the point in Figure 7.3 and, consequently, for the estimate of the corresponding B,E coordinates.
Estimation of $g_{l_{in}}$ **and** g_v - Figure 7.4C,D shows that segment lengths do not depend on centrifugal order, and that intermediate and terminal segments have approximately equal length. Similar findings have been obtained for Purkinje cell dendritic trees in mice [8] and in rat [19]. It is therefore reasonable to assume that segments in the Purkinje cells have not (or only moderately) undergone sustained elongation, and that the observed segment length distributions (almost) fully reflect the initial lengths at the time of their origin. According to this reasoning we can estimate the gamma distribution $g_{l_{in}}$ from the mean and standard deviation of the intermediate segment length distribution (Table 7.4). The length offset α_{in} has been estimated from the observed distribution to be α_{in}=0.7 μm.

Diameter parameters - Segment diameters can be assigned according to the procedure, described in section 2.2 with parameter values $\overline{e} = 2.0$, $\sigma_e = 0.3$, $\overline{d_t} = 1.1$ μm and $\sigma_{d_t} = 0.1$. [2])

TABLE 7.5
Optimized values for growth parameters to match the statistical shape properties of guinea pig Purkinje cell dendritic trees, given in Table 7.4. Parameters B, E, and S define the branching process, and $\alpha_{l_{in}}$, $\overline{l_{in}}$ and $\sigma_{l_{in}}$ define the gamma distribution for the initial segment lengths.

Growth parameters					
B	E	S	$\alpha_{l_{in}}$	$\overline{l_{in}}$	$\sigma_{l_{in}}$
95	0.69	-0.14	0.7 μm	10.63	7.53

Examples of trees, produced with the above estimates for the growth parameters (Table 7.5) are given in Fig. 7.6.

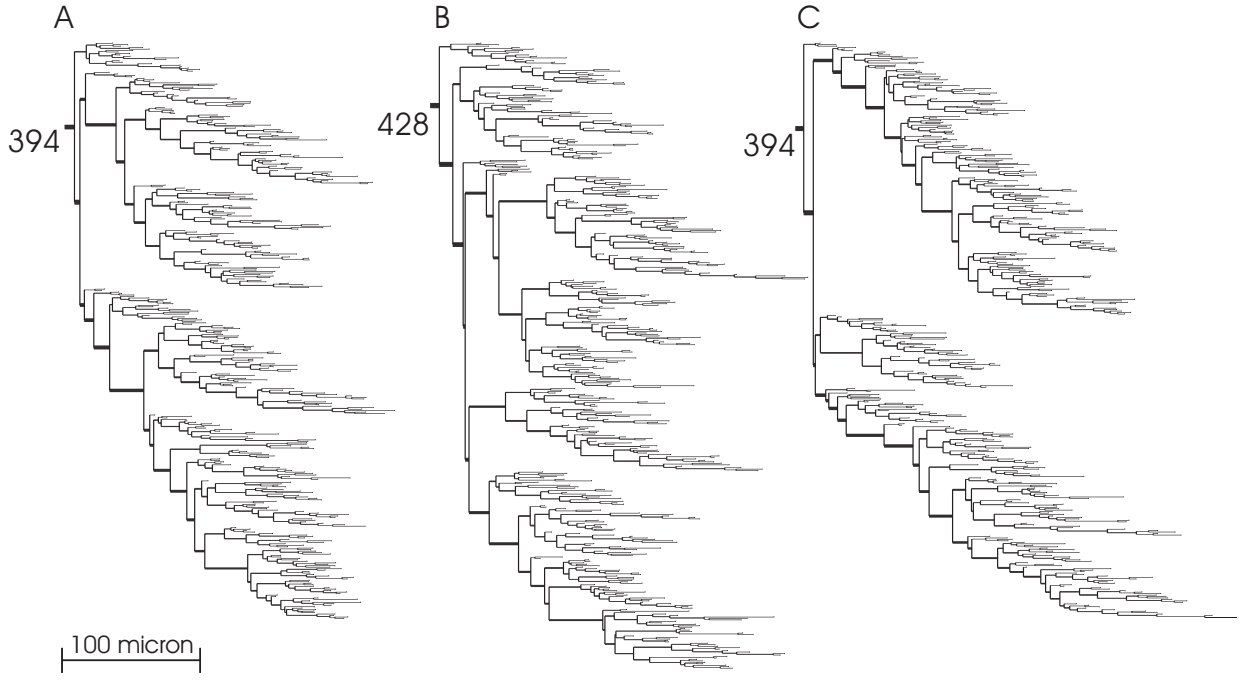

Figure 7.6 Examples of trees randomly produced by the growth model for parameter values, optimized for guinea-pig cerebellar Purkinje cells, as given in Table 7.5. Note that the diameters of the branches are not produced by this model, but randomly assigned according the procedure, described in Section 2.2.

Statistical properties of model-generated trees. Statistical properties of tree shapes, obtained by simulating 100 trees, are given in the 4th and 5th column of Table 7.4. An

excellent matching is shown in both the mean and standard deviation of the different shape parameters between the modeled and observed dendritic trees. Also the shapes of the distributions closely match, as is shown in Fig. 7.7 for the length distributions of intermediate and terminal segments.

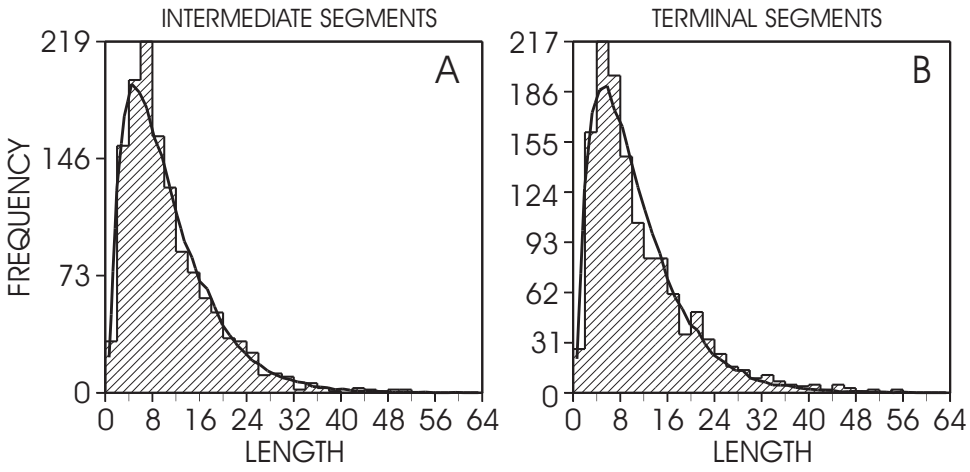

Figure 7.7 Comparison of (A) intermediate and (B) terminal segment length distributions of observed guinea pig Purkinje cells (hatched histograms) and model generated trees (continuous lines) for the parameter values given in Table 7.4.

7.1.6 Discussion

The two examples discussed have shown that the model for dendritic outgrowth is able to reproduce dendritic complexity, as measured by many geometrical properties to a high degree of correspondence. The basic assumptions are (1) randomness and (2) independence in branching and elongation. The modal shape of the intermediate segment length distributions could be described by dividing the elongation process into a first phase associated with branching events, and implemented in the model by the assignment of an initial length to newly formed daughter segments, and a second phase of sustained elongation. guinea pig Purkinje cell segment lengths turned out to be well described by the initial segment length assignments only. In contrast, rat pyramidal cell basal dendrites required, in addition to the initial segment length assignments there to be sustained elongation (with different rates for the first period of elongation and branching, and a second period of elongation only). The shape characteristics of the guinea pig Purkinje cells were based on dendritic reconstructions of only three cells. The empirical data for the mean and standard deviation of the degree, asymmetry index and total length consequently have modest stability and this could be the explanation for the difference in total length standard deviation between observed and modeled trees (Table 7.4).

The description of dendritic outgrowth as a stochastic process, defined by branching and elongation probabilities, is the reflection of a complex of molecular, biochemical and cellular processes. It is therefore surprising that a limited set of growth rules and parameters (especially in the case of the Purkinje cells) suffices to describe dendritic complexity with such a high level of accuracy. The phenomenological approach, along with the quantified probability

functions presented here, are first steps towards a further quantification of these processes underlying neurite outgrowth and neuronal morphogenesis.
The model is useful, since it can produce any number of dendritic trees with realistic variations in the number of segments, topological structure and intermediate and terminal segment lengths. Segment diameters are assigned using a branch power rule. These model dendrites can then be used in neural simulators for studying structure-function relationships in dendrites (see Chapters 8 and 9).

7.2 COMPETITION FOR NEUROTROPHIC FACTOR IN THE DEVELOPMENT OF NERVE CONNECTIONS

The development of connections between neurons and their target cells often involves an initial stage of hyperinnervation followed by elimination of axons. [23] In some cases, elimination continues until the target is innervated by just a single axon, whereas in most other cases, several innervating axons remain. An example of single innervation is the innervation of skeletal muscle fibres (for review see e.g. [24]). The cells that act as targets for the innervating axons appear to release limited amounts of "neurotrophic" factors, which are taken up by the axons via specific receptors at their terminals and which affect the growth and branching of the axons (for reviews see e.g. [25, 26]). An important class of neurotrophic factors is the neurotrophin family, with NGF (nerve growth factor) as its best characterized member.
Competition among innervating axons for neurotrophic factors is thought to be involved in axonal elimination and the generation of different patterns of innervation. [23] There is, however, little understanding of the nature of the competitive process and the underlying mechanisms. Computational models of activity-dependent development of nerve connections (e.g. of the formation of ocular dominance columns) typically enforce competition rather than model it explicitly (for a review see [27]). The first way in which this can be done is to enforce synaptic normalization. Consider n synapses, with efficacies s_i, impinging upon a given postsynaptic cell. Then, synaptic normalization is the constraint that $\sum_i^n s_i^p = K$, where K is some constant and p is usually taken to be 1 or 2. Following a phase of Hebbian learning, which changes the values of s_i, the new efficacies are forced to satisfy the normalization constraint.
A second approach is that of Bienenstock *et al.*, which does not impose synaptic normalization. [28] Here, a modified Hebb rule is used, which has the effect that inputs driving a postsynaptic cell below/above a certain threshold firing level cause a decrease/increase in synaptic efficacy. The threshold itself is a time-averaged function of the activity of the postsynaptic cell. This modified Hebb rule results in temporal competition between input patterns, rather than spatial competition between different sets of synapses.
In most existing models of the development of nerve connections that do try to explicitly model the putative underlying mechanism, competition is based on a fixed amount of neurotrophin that becomes partitioned among the individual synapses or axons, i.e. there is no production, decay, and consumption of the neurotrophin. (e.g. [29, 30, 31, 32, 33]) This

assumption is biologically not very realistic. Our approach, similar to that of Jeanprêtre *et al.* [34] in a model for the development of single innervation, considers the production and consumption of neurotrophin. By formulating a model that incorporates the dynamics of neurotrophic signalling (such as release of neurotrophin, binding kinetics of neurotrophin to receptor, and degradation processes) and the effects of neurotrophins on axonal growth and branching, competitive interactions emerge naturally. Our approach has similarities to that of Elliott and Shadbolt, although they do not model all the processes involved in a dynamic fashion (e.g. neurotrophin release and binding kinetics). [35]

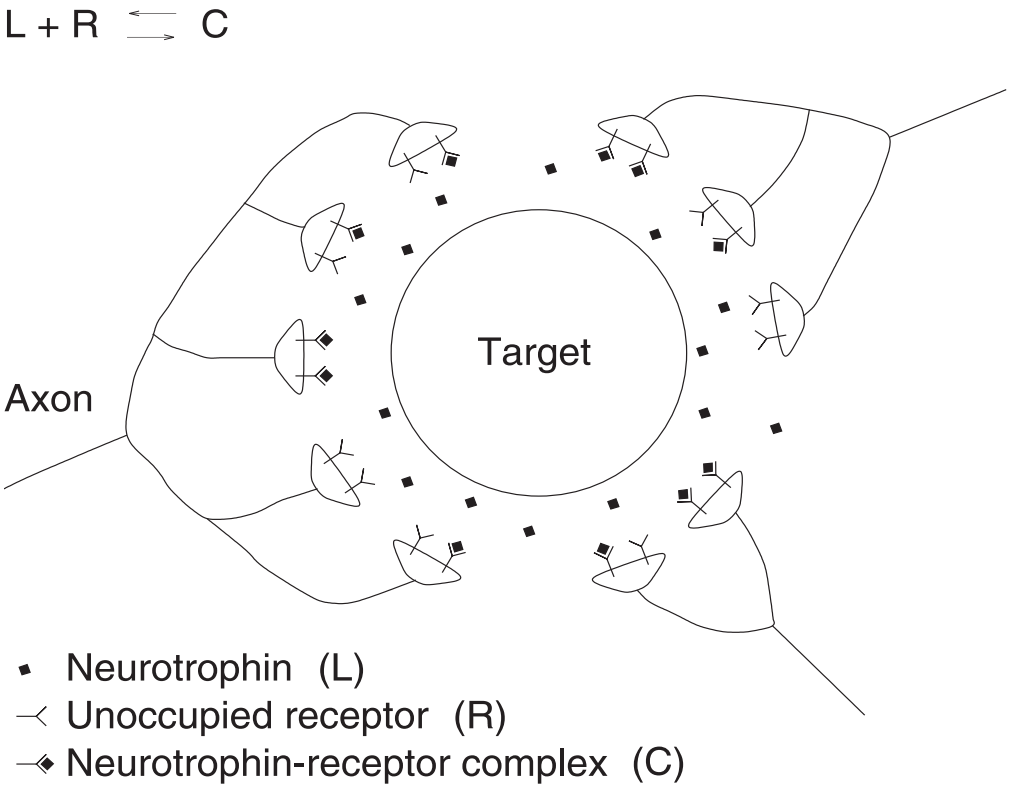

Figure 7.8 Single target with three innervating axons. The target releases neurotrophin that is bound by neurotrophin receptors at the axon terminals.

7.2.1 The model

The simplest situation in which we can study axonal competition is a single target at which there are a number of innervating axons each from a different neuron. Each axon has a number of terminals, on which the neurotrophin receptors are located (Fig. 7.8). In order to model competition, we break it down into a number of subprocesses. First, neurotrophin needs to be released by the target into the extracellular space. From there, it will be removed partly by degradation and diffusion and partly by binding to the neurotrophin receptors at the terminals of the innervating axons. The binding of neurotrophin to its receptor is a reversible reaction: the forward reaction produces the neurotrophin-receptor complex, and the backward reaction dissocates the complex back into neurotrophin and unoccupied receptor. The neurotrophin-receptor complex is then taken up by the axons and is also subject to degradation. Receptor as

well as neurotrophin are thereby removed. Therefore, we also need to consider the insertion of new receptors into the axon terminals, as well as turnover of unoccupied receptors. Finally, the growth and branching of each axon is affected by the amount of bound neurotrophin (neurotrophin-receptor complex) the axon has across its terminals.

7.2.1.1 Release and removal of neurotrophin

Because the binding of neurotrophin to receptor is what triggers the biological response, we describe, for each axon i, the time-dependent change of the axon's total amount of neurotrophin-receptor complex. The total amount of neurotrophin-receptor complex an axon has over all its terminals, C_i for axon i, increases by binding of neurotrophin to receptor, and decreases by dissociation and degradation. Thus, for the rate of change of C_i, we can formulate the following differential equation:

$$\frac{dC_i}{dt} = (k_{a,i} L R_i - k_{d,i} C_i) - \rho_i C_i, \tag{7.6}$$

where L is the extracellular concentration of neurotrophin, R_i is the total number of unoccupied receptors which axon i has over all its terminals, $k_{a,i}$ and $k_{d,i}$ are the respective association and dissociation constants of the reversible binding of neurotrophin to receptor, and ρ_i is the rate constant for degradation of the complex.
The total number of unoccupied receptors and the concentration of neurotrophin in the extracellular space are not constants but rather change in time. The total number of unoccupied receptors that an axon has over all its terminals, R_i for axon i, increases by the insertion of new receptors into the terminals as well as by dissociation of the neurotrophin-receptor complex; it decreases by the binding of neurotrophin to receptor and by receptor turnover. Thus,

$$\frac{dR_i}{dt} = \phi_i - \gamma_i R_i - (k_{a,i} L R_i - k_{d,i} C_i), \tag{7.7}$$

where ϕ_i is the rate of insertion of new receptors and γ_i is the rate constant of turnover.
The concentration of neurotrophin in the extracellular space, L, increases by the release of neurotrophin from the target and by the dissociation of neurotrophin-complex into neurotrophin and receptor; it decreases by the binding of neurotrophin to receptor and by degradation. Thus,

$$\frac{dL}{dt} = \sigma - \delta L - \sum_{i=1}^{n} (k_{a,i} L R_i - k_{d,i} C_i)/v, \tag{7.8}$$

where σ is the rate of release of neurotrophin, δ is the rate constant for degradation, n is the total number of innervating axons, and v is the volume of the extracellular space (L is a concentration, while R_i and C_i are defined as amounts). The rate of release of neurotrophin, σ, could depend on the level of electrical activity in the target.
Equations (7.6) and (7.7) are similar to the ones used in experimental studies for analysing the cellular binding, internalization and degradation of polypeptide ligands such as neurotrophins. (e.g. [36])

7.2.1.2 Axonal growth

The binding of neurotrophin to receptor triggers the biological response. Many studies have shown that neurotrophins locally increase the arborization of axons which will consequently cause an increase in the number of axon terminals. (e.g. [37]) It is reasonable to assume that increasing the number of axon terminals, on whichthe neurotrophin receptors are located, will increase the axon's total number of neurotrophin receptors. Other effects induced by neurotrophins that are likely to increase the total number of axonal neurotrophin receptors are (i) increasing the size of axon terminals (e.g. [38]) and (ii) upregulating the density of neurotrophin receptors (e.g. [39]).

In order for the total number of receptors to be able to increase in response to neurotrophins, the total number of unoccupied receptors that is inserted into the axon per unit time, ϕ_i, must increase in response to bound neurotrophin. We assume that the larger the amount of bound neurotrophin, C_i, the larger ϕ_i will be. That is, ϕ_i is an increasing function, $f_i(C_i)$, of the amount of bound neurotrophin, C_i. We call funtion $f_i(C_i)$ the growth function. Compared to the dynamics of the other processes involved, axonal growth takes place on a relatively slow time scale. To account for this, ϕ_i must lag behind its 'target' value given by $f_i(C_i)$. This lag can be modelled by the following differential equation:

$$\tau \frac{d\phi_i}{dt} = f_i(C_i) - \phi_i. \tag{7.9}$$

where the time constant τ of growth is of the order of days. The value of ϕ_i will follow changes in $f_i(C_i)$ (as a result of changes in C_i) with a lag; at steady-state, $\phi_i = f_i(C_i)$.

The precise form of the growth function, $f_i(C_i)$, is not known; we therefore use a general increasing function that can admit a range of different forms depending on its parameters. The effects of the form of the growth function on competition can then be studied. We use the general growth function

$$f_i(C_i) = \frac{\alpha_i C_i^m}{K_i^m + C_i^m}. \tag{7.10}$$

This is an increasing function that saturates towards a maximum, α_i. Parameter K_i is the value of C_i at which the response is half its maximum. Using this general growth function, we can distinguish a number of different classes of growth functions (Fig. 7.9).

Class O: for $m = 0$, $f_i(C_i)$ is a constant ($f_i(C_i) = \alpha_i/2$) and independent of the level of bound neurotrophin, C_i.

Class I: for $m = 1$ and large K_i ($K_i \gg C_i$), growth is linear over a large range of C_i ($f_i(C_i) \approx \alpha_i C_i/K_i$).

Class II: for $m = 1$ and smaller values of K_i ($K_i \not\gg C_i$), the growth function is a Michaelis-Menten function ($f_i(C_i) = \alpha_i C_i/(K_i + C_i)$) (see Chapter 2).

Class III: for $m = 2$ the growth function is a Hill function ($f_i(C_i) = \alpha_i C_i^2/(K_i^2 + C_i^2)$), which is sigmoidal.

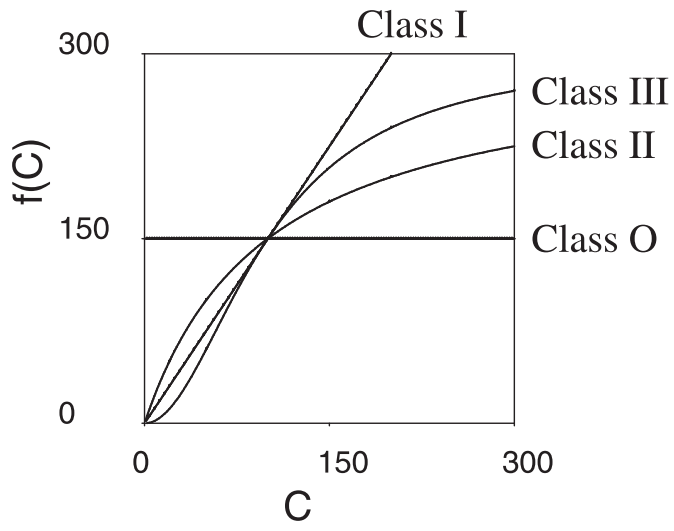

Figure 7.9 Growth function $f(C) = \alpha C^m/(K^m + C^m)$ for the different classes described in the text. For class O, $\alpha = 300$; for class I, $\alpha/K = 1.5$; for classes II & III, $\alpha = 300$ and $K = 100$.

Within each class of growth function, the specific values of the parameters (α_i and K_i), as well as those of the other parameters, may differ among axons. Various factors in the innervating axon, some dependent on, and some independent of its electrical activity, may influence the values of these parameters. For example, the finding that increased presynaptic electrical activity increases the number of neurotrophin receptors (e.g. [40]) implies that increased electrical activity affects growth (*i.e.* higher α_i or lower K_i) or neurotrophic signalling (*e.g.* lower γ_i) or both. As the level of electrical activity and other factors can vary among innervating axons, there will be variations in parameter values among axons.
The whole model thus consists of three differential equations for each axon i (eqns (7.6), (7.7), and (7.9)) and one equation for the neurotrophin concentration (eqn (7.8)). By means of numerical simulations and mathematical analysis, we can examine the outcome of the competitive process. Axons that at the end of the competitive process have no neurotrophin ($C_i = 0$; equivalent to $\phi_i = 0$) are assumed to have withdrawn or died, while axons that do have neurotrophin ($C_i > 0$; equivalent to $\phi_i > 0$) are regarded as having survived.

7.2.2 Units and parameter values

All parameters in the model have a clear biological interpretation. For the numerical simulations, the parameter values were taken from the data available for NGF. Because the high affinity NGF receptor mediates the biological response, the association and dissociation constants of this receptor were taken: $k_a = 4.8 \times 10^7$ [M^{-1} s^{-1}], $k_d = 1.0 \times 10^{-3}$ [s^{-1}]. [41] The rate constant for the turnover of receptor, γ, was calculated from the receptor half-life [42]; $\gamma = 2.7 \times 10^{-5}$ [s^{-1}]. The rate constant for the degradation of neurotrophin-receptor complex, ρ, was calculated from the half-life of complex [43]; $\rho \approx 2.0 \times 10^{-5}$ [s^{-1}]. The rate constant for degradation of neurotrophin in the extracellular space, δ, was estimated using data on neurotrophin concentration changes following blockade of axonal transport (as in [34]); $\delta \approx 1.0 \times 10^{-5}$[$s^{-1}$]. The standard value used in the model for the rate of release of neurotrophin was set at $\sigma \approx 2.0 \times 10^{-16}$ [M s^{-1}], which is well within the range of values

given in [44, 34]. Based on data on the time course of the growth of the number of receptors τ was set at 2 days. [45] Parameter v, the volume of the extracellular space around the target cell in which neurotrophin is released, acts as a scale parameter and was set at 1.7×10^{-11} [l].
The values of R_i, C_i, and K_i are in [number of molecules]; the value of L in [M] (= [mol l^{-1}]). The values of α_i and ϕ_i are in [number of molecules h^{-1}]. Time is in hours [h]. Only the value of α_i varies among axons. Unless otherwise indicated, the initial value of all ϕ_i is 10.0 [molecules h^{-1}]. The initial values of R_i, C_i and L are such that when keeping all ϕ_i at their initial value, the system is in equilibrium.

7.2.3 Examples of results and predictions

For an extensive overview of the results of the model, see [46]. Here we restrict ourselves to a few examples. The model (with growth functions of classes II and III) accounts for the experimental finding that increasing the amount of neurotrophin increases the number of surviving axons. (e.g. [47, 48]) In the model, elimination of axons takes place until either one or several axons survive, depending on (among other parameters) the rate of release of neurotrophin, σ: the larger σ, the more axons survive (Fig. 7.10a,b).
The axons having a survival advantage are the ones with the highest value for the quantity β_i defined as $(k_{a,i}(\alpha_i/K_i - \rho_i))/(\gamma_i(k_{d,i} + \rho_i))$, which we interpret as the axon's competitive strength. Because β_i contains parameters that may be affected by the axon's level of electrical activity (e.g. α_i), the axons having a survival advantage will be the most active ones provided that variations due to other factors do not predominate.
In agreement with the model, in skeletal muscle, stable states of single and multiple innervation can coexist, as with class III of the growth function (Fig. 7.10c). Persistent multiple innervation is found in partial denervation experiments after reinnervation and recovery from prolonged nerve conduction block. [49] In terms of the model, conduction block changes the competitive strengths of the axons, which changes the sizes of the basins of attractions of the different equilibria. This can cause the system to go to an equilibrium of multiple innervation, while under normal conditions single innervation develops. When the conduction block is removed, the system will remain in the basin of attraction of the multiple innervation equilibrium, i.e. multiple innervation persists.
Our analysis suggest that of the many axonal features that change during growth in response to neurotrophin (degree of arborization and, consequently, number of axon terminals; size of terminals; and density of receptors) the consequent change in the axon's total number of neurotrophin receptors, changing its capacity for removing neurotrophin, is what drives the competition. The model predicts that axons that are in the process of being eliminated will have a relatively small number of neurotrophin receptors.
The type of dose-response relationship between neurotrophin and total number of neurotrophin receptors (i.e. the growth function), which is crucial in our model for determining what patterns of innervation can develop, can be determined experimentally *in vitro* by measuring, for different concentrations of neurotrophin in the medium, the total number of terminals of an axon or, more specifically, the axon's total number of neurotrophin receptors (for details see [46]). The model predicts that the type of growth function will determine the relationship between the concentration of neurotrophin and the number of surviving axons.

For example, the smaller the value of K_i, the lower the concentration of neurotrophin needed to rescue more axons (Fig. 7.10d).

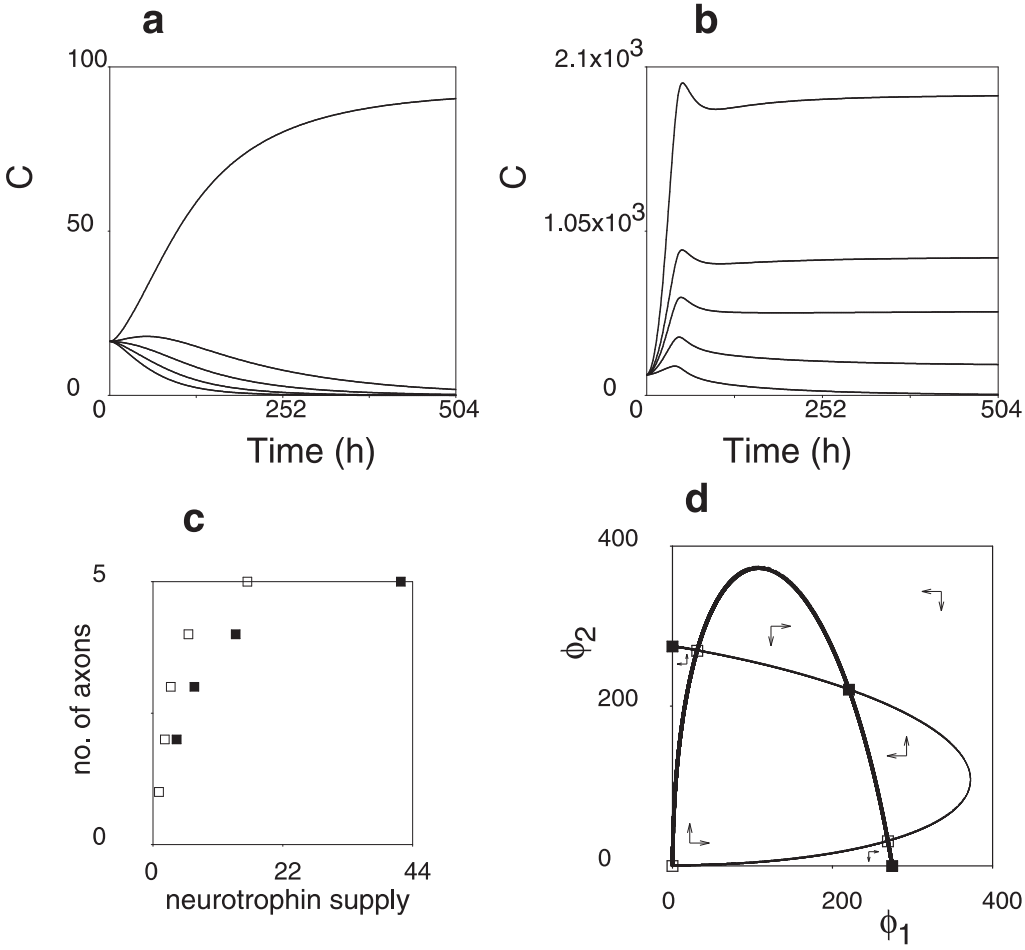

Figure 7.10 Results with class II of the growth function (**a,b,c**). **a.** Single innervation. The axon with the highest value of α_i among the initial 5 axons survives. $\alpha_1 = 700$, $\alpha_2 = 400$, $\alpha_3 = 300$, $\alpha_4 = 200$, $\alpha_5 = 100$ and $K = 500$. **b.** Multiple innervation with a rate of release of neurotrophin, σ, that is 35 times higher than the standard value. Other parameter values as in **a**. **c.** Relationship between the rate of release of neurotrophin (in units of the standard value) and the number of axons with $C_i > 10$ at $t = 504$, for $K = 500$ (filled squares) and $K = 150$ (open squares). Other parameter values as in **a**. **d.** Coexistence of equilibrium points of single and multiple innervation, in a system of two innervating axons ($n = 2$), with a class III growth function. The variables $\{R_i, C_i, i = 1, 2\}$ and L are at quasi-steady state. The bold line depicts the solutions of the equation $\frac{d\phi_1}{dt} = 0$ and the light line those of $\frac{d\phi_2}{dt} = 0$. (the lines $\phi_1 = 0$ and $\phi_2 = 0$ are also solutions of $\frac{d\phi_1}{dt} = 0$ and $\frac{d\phi_2}{dt} = 0$, respectively, but are not drawn). The intersection points of these nullclines are the equilibrium points of the system. Vectors indicate direction of change. Filled square indicates stable equilibrium point, and open square unstable equilibrium point (Note that $\phi_i > 0 \Leftrightarrow C_i > 0$ (axon i present) and $\phi_i = 0 \Leftrightarrow C_i = 0$ (axon i eliminated)). The stable equilibrium point at $(\phi_1 = 0, \phi_2 = 0)$ is not indicated as it is too close to another, unstable point. Which of the stable equilibria will be reached depends on the initial values of ϕ_i, and the sizes of the basins of attraction of the equilibria, which are sensitive to the values of the competitive strengths, β_i. Parameters: $\alpha_1 = \alpha_2 = 300$, $K = 30$.

7.2.4 Conclusions

Our model of competition links the formation of nerve connections with the underlying actions and biochemistry of neurotrophins. The model accounts for the development of single and multiple innervation, as well as several other experimental findings, and makes testable predictions. Although the parameter values were taken from the data available for NGF, mathematical analysis shows that our results are general and do not depend on specific choices of the parameter values. [46]

The model can be extended in several ways. In reality, axons can have more than one target. In the model, the rate of insertion of receptors could then be different for branches innervating different targets. This will cause also competition within axons between different branches in addition to competition among axons. (see also [30, 31])

In the present model, we have assumed that the concentration of neurotrophin is homogeneous in the extracellular space that surrounds the target; in other words, all innervating axons 'sense' the same concentration. This assumption may not be realistic, especially if the target is large (e.g. a neuron with a large dendritic tree, onto which the axons impinge). This can be taken into account in our model by modelling the extracellular space as a collection of 'compartments', into which neurotrophin is released locally from the target. Some of the compartments will have an innervating axon, which removes neurotrophin molecules locally. In addition, there will be diffusion of neurotrophin between compartments (see Chapter 3). For preliminary results of such a model, see [50].

Acknowledgments

We are very grateful to Dr. M.A. Corner for his critical comments and improvements of the manuscript.

Bibliography

[1] Burke, R. E., Marks, W. B., and Ulfhake, B., A parsimonious description of motoneuron dendritic morphology using computer simulation, *J. Neurosc.*, 12, 2403, 1992.

[2] Hillman, D. E., Parameters of dendritic shape and substructure: Intrinsic and extrinsic determination?, in *Intrinsic Determinants of Neuronal Form and Function*, Lasek, R.J., Black, M. M., Eds., A.R. Liss, New York, 1988, 83.

[3] Tamori, Y., Theory of dendritic morphology, *Physical Rev.*, E48, 3124, 1993.

[4] Ascoli, G., and Krichmar, J. L., L-Neuron: a modeling tool for the efficient generation and parsimonious description of dendritic morphology, *Neurocomputing*, (in press).

[5] Kliemann, W. A., Stochastic dynamic model for the characterization of the geometrical structure of dendritic processes, *Bull. Math. Biol.*, 49, 135, 1987.

[6] Uemura, E., Carriquiry, A., Kliemann, W., and Goodwin, J., Mathematical modeling of dendritic growth in vitro, *Brain Res.*, 671, 187, 1995.

[7] Letourneau, P. C., Kater, S. B., and Macagno, E. R., Eds., *The nerve growth cone*, Raven Press, New York, 1991.

[8] Sadler, M., and Berry, M., Morphometric study of the development of Purkinje cell dendritic trees in the mouse using vertex analysis, *J. Microsc.*, 131, 341, 1983.

[9] Horsfield, K., Woldenberg, M. J., and Bowes, C. L., Sequential and synchronous growth models related to vertex analysis and branching ratios, *Bull. Math. Biol.*, 49, 413, 1987.

[10] Van Pelt, J., Dityatev, A. E., and Uylings, H. B. M., Natural variability in the number of dendritic segments: Model-based inferences about branching during neurite outgrowth, *J. Comp. Neurol.*, 387, 325, 1997.

[11] Van Pelt, J., and Uylings, H. B. M., Natural variability in the geometry of dendritic branching patterns, In *Modeling in the Neurosciences: From Ionic Channels to Neural Networks*, Poznanski, R. R. (Ed.), Harwood Academic Publishers, Amsterdam, 1999, 79.

[12] Ireland, W., Heidel, J., and Uemura, E., A mathematical model for the growth of dendritic trees, *Neurosc. Lett.*, 54, 243, 1985.

[13] Nowakowski, R. S., Hayes, N. L., and Egger, M. D., Competitive interactions during dendritic growth: a simple stochastic growth algorithm, *Brain Res.*, 576, 152, 1992.

[14] Li, G.-H., and Qin, C.-D., A model for neurite growth and neuronal morphogenesis, *Math. Biosc.*, 132, 97, 1996.

[15] Van Veen, M. P., and Van Pelt, J., Neuritic growth rate described by modeling microtubule dynamics, *Bull. Math. Biol.*, 56, 249, 1994.

[16] Uylings, H. B. M., Van Pelt, J., Parnavelas, J. G., and Ruiz-Marcos, A., Geometrical and topological characteristics in the dendritic development of cortical pyramidal and nonpyramidal neurons, in *Progress in Brain Research, Vol. 102, The Self-Organizing Brain: From Growth Cones to Functional Networks*, Van Pelt, J., Corner, M. A., Uylings, H. B. M., and Lopes da Silva, F. H., Eds., Elsevier, Amsterdam, 1994, 109.

[17] Van Veen, M. P., and Van Pelt, J., Terminal and intermediate segment lengths in neuronal trees with finite length, *Bull. Math. Biol.*, 55, 277, 1993.

[18] Abramowitz, M., and Stegun, I. A., *Handbook of Mathematical Functions*, Dover, New York, 1970.

[19] Uylings, H. B. M., Ruiz-Marcos, A., and Van Pelt, J., The metric analysis of three-dimensional dendritic tree patterns: a methodological review, *J. Neurosc. Meth.*, 18, 127, 1986.

[20] Schierwagen, A. K., and Grantyn, R., Quantitative morphological analysis of deep superior colliculus neurons stained intracellularly with HRP in the cat, *J. Hirnforsch*, 27, 611, 1986.

[21] Larkman, A. U., Dendritic morphology of pyramidal neurones of the visual cortex of the rat: I. Branching patterns, *J. Comp. Neurol.*, 306, 307, 1991.

[22] Rapp, M., Segev, I., and Yarom, Y., Physiology, morphology and detailed passive models of guinea-pig cerebellar Purkinje cells, *J. Physiol.*, 474, 101, 1994.

[23] Purves, D., and Lichtman, J. W., *Principles of neural development*, Sunderland, Massachusetts: Sinauer, 1985.

[24] Sanes, J. R., and Lichtman, J. W., Development of the vertebrate neuromuscular junction, *Annu. Rev. Neurosci.*, 22, 389, 1999.

[25] Bothwell, M., Functional interactions of neurotrophins and neurotrophin receptors. *Ann. Rev. Neurosc.*, 18, 223, 1995.

[26] McAllister, A. K., Katz, L. C., and Lo, D.C., Neurotrophins and synaptic plasticity, *Annu. Rev. Neurosci.*, 22, 295, 1999.

[27] Miller, K. D., Synaptic economics: competition and cooperation in correlation-based synaptic plasticity, *Neuron*, 17, 371, 1996.

[28] Bienenstock, E. L., Cooper, L. N., and Munro, P. W., Theory for the development of neuron selectivity: orientation specificity and binocular interaction in visual cortex, *J. Neurosc.*, 2, 32, 1982.

[29] Bennett, M. R., and Robinson, J., Growth and elimination of nerve terminals at synaptic sites during polyneuronal innervation of muscle cells: a trophic hypothesis, *Proc. R. Soc. Lond. B*, 235, 299, 1989.

[30] Rasmussen, C. E., and Willshaw, D. J., Presynaptic and postsynaptic competition in models for the development of neuromuscular connections, *Biol. Cybern.*, 68, 409, 1993.

[31] Van Ooyen, A., and Willshaw, D. J., Poly-and mononeuronal innervation in a model for the development of neuromuscular connections, *J. Theor. Biol.*, 196, 495, 1999.

[32] Elliott, T., and Shadbolt, N. R., A mathematical model of activity-dependent anatomical segregation induced by competition for neurotrophic support, *Biol. Cybern.*, 75, 463, 1996.

[33] Harris, A. E., Ermentrout, G. B., and Small, S. L., A model of ocular dominance development by competition for trophic factor, *Proc. Natl. Acad. Sci. USA*, 94, 9944, 1997.

[34] Jeanprêtre, N., Clarke, P. G. H., and Gabriel, J.-P., Competitive exclusion between axons dependent on a single trophic substance: a mathematical analysis, *Math. Biosc.*, 133, 23, 1996.

[35] Elliott, T., and Shadbolt, N. R., Competition for neurotrophic factors: mathematical analysis, *Neural Computation*, 10, 1939, 1998.

[36] Wiley, H. S., and Cunningham, D. D., A steady state model for analyzing the cellular binding, internalization and degradation of polypeptide ligands, *Cell*, 25, 433, 1981.

[37] Cohen-Cory, S., and Fraser, S. E., Effects of brain-derived neurotrophic factor on optic axon branching and remodelling in *in vivo*, *Nature*, 378, 192, 1995.

[38] Garofalo, L., Ribeiro-da-Silva, A., and Cuello, C., Nerve growth factor-induced synaptogenesis and hypertrophy of cortical cholinergic terminals, *Proc. Natl. Acad. Sci. USA*, 89, 2639, 1992.

[39] Holtzman, D. M., Li, Y., Parada, L. F., Kinsman, S., Chen, C.-K., Valletta, J. S., Zhou, J., Long, J.B., and Mobley, W. C., p140^{trk} mRNA marks NGF-responsive forebrain neurons: evidence that *trk* gene expression is induced by NGF, *Neuron*, 9, 465, 1992.

[40] Birren, S. J., Verdi, J. M., and Anderson, D. J., Membrane depolarization induces p140$^{\mathrm{trk}}$ and NGF responsiveness, but not p75$^{\mathrm{LNGFR}}$, in MAH cell, *Science*, 257, 395, 1992.

[41] Sutter, A., Riopelle, R. J., Harris-Warrick, R. M., and Shooter, E. M., Nerve growth factor receptors. Characterization of two distinct classes of binding sites on chick embryo sensory ganglia cells, *J. Biol. Chem.*, 254, 5972, 1979.

[42] Zupan, A. A., and Johnson Jr., E. M., Evidence for endocytosis-dependent proteolysis in the generation of soluble truncated nerve growth factor receptors by A875 human melanoma cells, *J. Biol. Chem.*, 266, 15384, 1991.

[43] Layer, P. G., and Shooter, E. M., Binding and degradation of nerve growth factor by PC12 pheochromocytoma cells, *J. Biol. Chem.*, 258, 3012, 1983.

[44] Blöchel, A., and Thoenen, H., Characterization of nerve growth factor (NGF) release from hippocampal neurons: evidence for a constitutive and an unconventional sodium-dependent regulated pathway, *Eur. J. Neurosc.*, 7, 1220, 1995.

[45] Bernd, P., and Greene, L. A., Association of ^{125}I-nerve growth factor with PC12 pheochromocytoma cells. Evidence for internalization via high affinity receptors only and for long-term regulation by nerve growth factor of both high- and low-affinity receptors, *J. Biol. Chem.*, 259, 15509, 1984.

[46] Van Ooyen, A., and Willshaw, D. J., Competition for neurotrophic factor in the development of nerve connections, *Proc. R. Soc. Lond. B*, 266, 883, 1999.

[47] Albers, K. M., Wright, D. E., and Davies, B. M., Overexpression of nerve growth factor in epidermis of transgenic mice causes hypertrophy of the peripheral nervous system, *J. Neurosc.*, 14, 1422, 1994.

[48] Nguyen, Q. T., Parsadanian, A. S., Snider, W. D., and Lichtman, J.W., Hyperinnervation of neuromuscular junctions caused by GDNF overexpression in muscle, *Science*, 279, 1725, 1998.

[49] Barry, J. A., and Ribchester, R. R., Persistent polyneuronal innervation in partially denervated rat muscle after reinnervation and recovery from prolonged nerve conduction block, *J. Neurosc.*, 15, 6327, 1995.

[50] Van Ooyen, A., and Willshaw, D. J., Influence of dendritic morphology on axonal competition, in *Artificial Neural Networks* - ICANN'99, Institution of Electrical Engineers, London, 9th International Conference on Artificial Neural Networks, Edinburgh, September, 1999, 1000.